Research Article GU J Sci, Part A, 13(3): 1422-1433 (2026) 10.54287/gujsa.1999055

Gazi University
Journal of Science
PART A: ENGINEERING AND INNOVATION
http://dergipark.org.tr/gujsa

Investigation of Radiation Shielding Properties of Al 7075 Matrix B_4C/TiB_2 Reinforced Composites in Phy-x/PSD Program

Can YILDIRIM[1] Zübeyde ÖZKAN[2*] Ufuk TAŞCI[3] Uğur GÖKMEN[4]

1 Minerals and Boron Technology, Graduate School of Natural and Applied Sciences, Gazi University, 06560, Ankara, Türkiye
2 Graduate School of Natural and Applied Sciences, Gazi University, 06560, Ankara, Türkiye
3 Department of Mechanical Program, Gazi University, 06500, Ankara, Türkiye
4 Department of Metallurgical and Materials Engineering, Faculty of Technology, Gazi University, 06560, Ankara, Türkiye

Keywords

B_4C
TiB_2
Al 7075
Radiation Shielding

Abstract

This study investigated the radiation shielding performance of Al 7075 matrix composites reinforced with specific ratios (5-10-15%) of B_4C and TiB_2 ceramic reinforcement materials. Using Phy-x/PSD software, main radiation shielding parameters such as the mass attenuation coefficient (MAC) and linear attenuation coefficient (LAC) were analyzed for different MMC radiation shielding compositions. The primary objective of the study was to determine the radiation shielding performance of boron ore and its derivatives, which hold strategic importance for Türkiye, with the aim of expanding their application areas particularly in the defense industry and increasing their added value. It was observed that the addition of B_4C slightly reduced gamma shielding compared to the Al 7075 (S1) due to its effect of lowering the material's average atomic number (Z).

Cite

Yıldırım, C., Özkan, Z., Taşçı, U., & Gökmen, U. (2026). Investigation of Radiation Shielding Properties of Al 7075 Matrix B_4C/TiB_2 Reinforced Composites in Phy-x/PSD Program. *GU J Sci, Part A*, *13*(3), 1422-1433. doi:10.54287/gujsa.1999055

Author ID (ORCID Number)

0009-0006-0759-8086 Can YILDIRIM
0000-0003-2901-7749 Zübeyde ÖZKAN
0000-0002-8577-443X Ufuk TAŞCI
0000-0002-6903-0297 Uğur GÖKMEN

Article Process

Submission Date 20.07.2026
Revision Date 11.08.2026
Accepted Date 02.09.2026
Early Pub Date 29.09.2026
Published Date 30.09.2026

1. INTRODUCTION

The rising use of radiation technologies in fields such as nuclear energy, medicine, aerospace, and industrial radiography has heightened the need for advanced shielding materials to protect personnel and sensitive equipment from the harmful effects of ionizing radiation (particularly neutrons and gamma rays) (Hubbell & Seltzer, 2004; Knoll, 2010). The intensity of natural radiation is considerably lower than that obtained through artificial means. In high-tech aerospace and defense applications, prolonged exposure to ionizing radiation (e.g., gamma, alpha, beta) necessitates the development of structural shielding materials that provide long-term stability (Hubbell & Seltzer, 2004; Knoll, 2010; Albandar, 2019).

Materials traditionally used in radiation shielding, such as lead (Pb) or concrete, are inadequate in modern engineering fields particularly in aviation and mobile nuclear applications due to their high weight, toxicity, and limited mechanical strength (Sayyed et al., 2018). To address these weight limitations, metal matrix composites (MMCs) offer a highly practical approach by delivering robust radiation attenuation at a much

*Corresponding Author, e-mail: zubeydeozkan@gazi.edu.tr

This work is licensed under Creative Commons Attribution 4.0 International.

GU J Sci, Part A | 13(3) 1422-1433 (2026) | 10.54287/gujsa.1999055

lower density (Dai et al., 2013; Akkas et al., 2015). Thanks to an exceptional balance of low density and high specific strength, aluminum alloys serve as the primary matrix in MMC manufacturing (Miller et al., 2000; Starke & Staley, 2011). Among these, the Al 7075 alloy is widely preferred in the aerospace and defense sectors where extreme toughness is required (Heinz et al., 2000; Williams & Starke, 2003). However, the low atomic number (Z) of aluminum fundamentally restricts its ability to attenuate radiation (Sayyed et al., 2018).

A combination of functionally reinforcing particles offers an effective solution to overcome this capacity limitation. The incorporation of boron carbide (B_4C) enhances the neutron absorption cross section, whereas TiB_2 contributes to both elevated-temperature stability and effective photon attenuation (Akkurt et al., 2010; Toptan et al., 2010; Akkas et al., 2015). The combined use of these reinforcing particles simultaneously improves both the radiation shielding efficiency and the mechanical resistance of the composite against wear and deformation (Canakci & Arslan, 2012; Şakar et al., 2020). Research indicates that the neutron shielding capacity of aluminum matrices scales effectively with the amount of B_4C added, yielding substantially higher attenuation coefficients at greater boron levels (Dai et al., 2013; Akkas et al., 2015). Although B_4C guarantees high neutron absorption, it couldn't act as a comprehensive shield on its own therefore its weak gamma attenuation. The addition of high-density phases such as TiB_2 successfully compensates for this weakness, providing highly effective gamma resistance (Singh & Badiger, 2013; Agar et al., 2019). The low density, high corrosion resistance, and structural integrity of the AMCs formulated in this study demonstrate critical performance compatibility as defined by the modern aerospace and nuclear industries (Chen et al., 2025).

Theoretically investigated the radiation shielding (neutron and gamma rays) performance of Al 7075 composites reinforced with varying weight ratios of B_4C/TiB_2 ceramics, aiming to contribute to the development of next-generation lightweight composites that provide both structural strength and versatile radiation shielding.

2. MATERIALS AND THEORETICAL ANALYSIS (PHY-X/PSD)

Table 1 shows the weight percentage distribution of the elements in Al 7075 alloy.

Table 1. *Chemical composition of 7075 aluminum alloy*

Element	Symbol	Concentration (wt%)
Aluminum	Al	89.60
Magnesium	Mg	2.50
Zinc	Zn	5.60
Copper	Cu	1.60
Manganese	Mn	0.06
Chromium	Cr	0.23
Silicon	Si	0.10
Iron	Fe	0.20
Titanium	Ti	0.04
Others (Trace*)	-	0.07
Total	-	100.00

The systematic coding scheme, weight percentage (%) compositions, and density values of the single-reinforced and hybrid-reinforced composite specimens based on the Al 7075 matrix designed within the scope

GU J Sci, Part A | 13(3) 1422-1433 (2026) | 10.54287/gujsa.1999055

of this study are presented in Figure 1. The density values of the Al 7075, B_4C, and TiB_2 materials used in the analysis are 2.81 g/cm^3, 2.52 g/cm^3, and 4.52 g/cm^3, respectively (Shackelford & Alexander, 2001).



Figure 1. *Systematic representation and nomenclature of B_4C and TiB_2 reinforced Al 7075 matrix composite samples.*

The radiation interactions of the samples were determined using the Phy-x/PSD software. It has been reported in the literature that this software demonstrates over 99% agreement with the National Institute of Standards and Technology (NIST) database for complex composite systems and produces results with high reliability (Şakar et al., 2020). The technical details of the parameters analyzed are as follows (Equations 1–5):

MAC (Mass Attenuation Coefficient): It is obtained by dividing the LAC by the material's density. This parameter is independent of density and is entirely related to the material's chemical composition and Z (Hubbell & Seltzer, 1995). Its unit is cm^2/g.

TVL (Tenth Value Layer): The shielding thickness required to reduce the intensity of radiation striking the material to 10% (i.e., one-tenth) (Knoll, 2010; Sayyed et al., 2018). Its unit is cm.

FNRCS (Fast neutron Cross Section): Represents the possibility that fast neutrons will interact with a material and be removed from the fast neutron flux (through moderation or absorption). In composites, it is calculated based on the weight fraction of each component (El-Khayatt, 2010). Its unit is cm^{-1}.

LAC (Linear Attenuation Coefficient): Represents the probability of attenuation of ionizing radiation per unit distance as it passes through a material due to photoelectric effects, Compton scattering, etc. It is directly dependent on the material's density and the incident radiation's energy (Knoll, 2010). Its unit is cm^{-1}.

GU J Sci, Part A | 13(3) 1422-1433 (2026) | 10.54287/gujsa.1999055

MFP (Mean Free Path): The average distance a radiation particle travels within a material between two successive interactions (collisions). A low MFP value indicates higher stopping power (Wood, 1982). Its unit is cm.

In the parameters given in Equations 1-5, I_o represents the initial photon intensity, I represents the attenuated photon intensity, μ represents the linear attenuation coefficient, μ_m represents the mass attenuation coefficient and x represents the material thickness.

$$\text{MAC} : \mu_m = \frac{\mu}{\rho} \tag{1}$$

$$\text{LAC} : \mu = ln\left(\frac{Io}{I}\right)\frac{1}{x} \tag{2}$$

$$\text{MFP} : \frac{1}{\mu} \tag{3}$$

$$\text{TVL} : \frac{ln(10)}{\mu} \tag{4}$$

$$\text{FNRCS} : \Sigma_R = \sum_i w_i \left(\frac{\Sigma_R}{\rho}\right)_i \tag{5}$$

3. RESULTS AND DISCUSSION

In this study, the shielding performance of composites (S1–S10) with an Al 7075 matrix and different ratios of B_4C/TiB_2 reinforcements against gamma and neutron radiation was theoretically investigated using the Phy-x/PSD software.

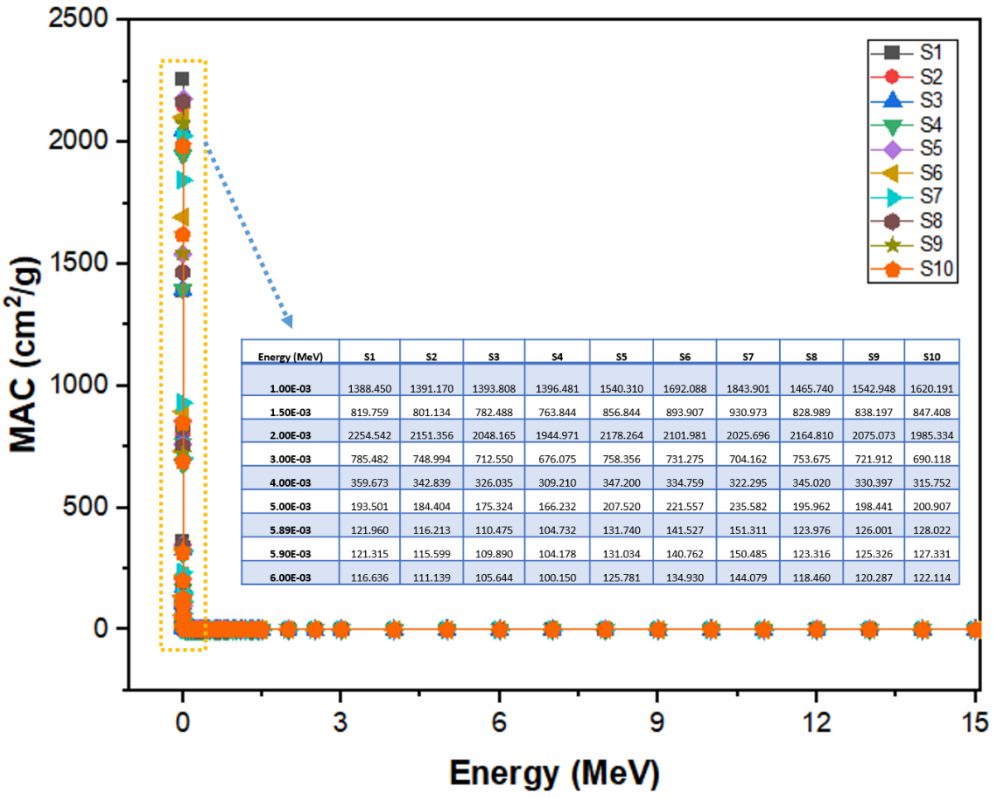
MAC

At low energies, photoelectric absorption dominates, and this process is directly proportional to the Z raised to the power of 4 to 5. At intermediate energies (Compton scattering), it depends on the mass number, and at high energies, it depends on pair production. When the MAC values computed for the specimens in the energy range of 0.015–15 MeV are investigated (Figure 2), it is noticed that the MAC performance for all materials attains its maximum level at low energies, however a sharp decrease occurs as the photon energy rises. This characteristic behavior is owing to the dominance of the photoelectric effect (PE) in the low-energy regions (E < 0.1 MeV) (Knoll, 2010). As is known, the probability of PE is proportional to the fourth or fifth exponential coefficient of the Z of the material (Knoll, 2010).

When the S1-S10 were compared, it was found that the addition of TiB_2 significantly improved the gamma shielding performance of Al 7075. Compared to the aluminum (Z=13) that forms the matrix, titanium (Z=22) has a much higher Z and therefore a larger photon interaction cross-section. In this context, sample S7, containing 15% TiB_2, showed the highest photon absorption and obtained the highest MAC values. Particularly in the absorption of low-energy photons, titanium's high atomic mass has maximized the shielding potential by increasing the matrix's effective atomic number (Z_{eff}) (Şakar et al., 2020).

GU J Sci, Part A | 13(3) 1422-1433 (2026) | 10.54287/gujsa.1999055

However, a decrease in gamma shielding performance was observed with an increase in B_4C reinforcement. The incorporation of elements with low Z, such as boron and carbon, reduces the material's average atomic weight. This situation has resulted in the S4 sample, containing 15% B_4C, exhibiting lower MAC values than the Al 7075 (S1) matrix without any reinforcement material. As noted in the literature, while lightweight element reinforcements provide advantages in neutron shielding, they create a limiting effect in stopping high-energy electromagnetic radiation due to the reduction in mass density (Sayyed et al., 2018). In the hybrid series consisting of samples S8, S9, and S10, it is observed that the low Z and density of B_4C are balanced by the high atomic number-density ratio of TiB_2. The hybrid samples exhibited a cumulative attenuation profile located in the mid-band between S4 and S7 in the MAC spectrum. Sample S10 compensated for the performance loss caused by B_4C thanks to the high absorption capacity of TiB_2, establishing an optimal balance between shielding performance and lightness which is highly consistent with the synergistic effects of high-density reinforcements reported in the literature (Singh & Badiger, 2013; Agar et al., 2019; Şakar et al., 2020).



Energy (MeV)	S1	S2	S3	S4	S5	S6	S7	S8	S9	S10
1.00E-03	1388.450	1391.170	1393.808	1396.481	1540.310	1692.088	1843.901	1465.740	1542.948	1620.191
1.50E-03	819.759	801.134	782.488	763.844	856.844	893.907	930.973	828.989	838.197	847.408
2.00E-03	2254.542	2151.356	2048.165	1944.971	2178.264	2101.981	2025.696	2164.810	2075.073	1985.334
3.00E-03	785.482	748.994	712.550	676.075	758.356	731.275	704.162	753.675	721.912	690.118
4.00E-03	359.673	342.839	326.035	309.210	347.200	334.759	322.295	345.020	330.397	315.752
5.00E-03	193.501	184.404	175.324	166.232	207.520	221.557	235.582	195.962	198.441	200.907
5.89E-03	121.960	116.213	110.475	104.732	131.740	141.527	151.311	123.976	126.001	128.022
5.90E-03	121.315	115.599	109.890	104.178	131.034	140.762	150.485	123.316	125.326	127.331
6.00E-03	116.636	111.139	105.644	100.150	125.781	134.930	144.079	118.460	120.287	122.114

Figure 2. *Photon energy dependent MAC values of S1–S10*

MFP

This parameter (MFP = 1/LAC), which is theoretically inversely proportional to the LAC, is a direct indicator of the stopping power of the shielding material; in radiation shielding material designs, the goal is to minimize this value (Wood, 1982). An examination of the MFP graphs presented in Figure 3 and Table 2 reveals that the MFP values of all samples rise with rising photon energy. Owing to the high probability of photon-matter interaction in the low-energy regions, MFP values are at minimum levels; however, as the penetration

GU J Sci, Part A | 13(3) 1422-1433 (2026) | 10.54287/gujsa.1999055

capability of photons increases at higher energies, these values potentially rise and plateau in the high-energy regions (Knoll, 2010).

When evaluating the performance differences among the samples, the S7 sample reinforced with 15% TiB_2 demonstrated the most effective shielding performance by achieving the lowest MFP values across all energy ranges. The addition of TiB_2 maximized the LAC value by increasing both the density and the content of high Z (Z=22) elements in the composite material, which minimized the MFP value of photons. This result demonstrates that the S7 sample can be designed with a much thinner plate thickness compared to other compositions to provide the same protection factor, which is consistent with the shielding behavior of high-density materials reported in the literature (Sayyed et al., 2018).

Table 2. *MFP values of samples depending on varying energies.*

Energy (MeV)	S1	S2	S3	S4	S5	S6	S7	S8	S9	S10
1.50E-02	0.027	0.028	0.030	0.032	0.025	0.024	0.022	0.027	0.026	0.026
2.00E-02	0.060	0.063	0.067	0.071	0.056	0.053	0.050	0.060	0.059	0.059
2.21E-02	0.079	0.084	0.089	0.094	0.075	0.070	0.066	0.079	0.079	0.078
2.21E-02	0.079	0.084	0.089	0.094	0.075	0.070	0.066	0.079	0.079	0.078
2.31E-02	0.090	0.095	0.100	0.106	0.085	0.080	0.075	0.089	0.089	0.089
2.50E-02	0.112	0.118	0.125	0.132	0.105	0.099	0.094	0.111	0.111	0.110
2.55E-02	0.118	0.125	0.132	0.139	0.111	0.105	0.099	0.118	0.117	0.117
2.63E-02	0.129	0.136	0.144	0.152	0.122	0.115	0.108	0.129	0.128	0.127
3.00E-02	0.184	0.194	0.204	0.216	0.173	0.164	0.155	0.183	0.182	0.181

In contrast, the S4 sample (15% B_4C), which exhibits poorer shielding performance against gamma rays due to the presence of low Z elements such as boron and carbon in its structure, yielded the highest MFP values. Consistent with literature data, this finding demonstrates that light element reinforcements reduce the probability of photon interaction and require a thicker shield geometry for the same level of radiation shielding (Hubbell & Seltzer, 1995). In the hybrid series (S8–S10), the MFP values were optimized between these two extreme values due to the balanced effect of the reinforcement phases on density and atomic number.

LAC

When examining Figure 4, it can be seen that the LAC values of all samples (S1–S10) reach their maximum in the low-energy regions (especially <0.1 MeV) and decrease rapidly as the energy increases. Among the samples, sample S7 (15% TiB_2) has the highest LAC values across the entire energy spectrum. The main reason for this is that titanium (Z=22) has a higher atomic number than aluminum (Z=13), the matrix material, and increases the overall bulk density of the alloy. The LAC values of sample S4 (15% B_4C) are even lower than

GU J Sci, Part A | 13(3) 1422-1433 (2026) | 10.54287/gujsa.1999055

those of Al 7075 (S1), which does not contain reinforcement material. The low-density and low-atomic-number structure of boron and carbon reduces the stopping power by decreasing the probability of interaction per unit volume. Although all curves appear close to each other at energies in the main graph, the graph given in the 0.1 MeV-0.2 MeV energy range highlights the differences in this energy range.

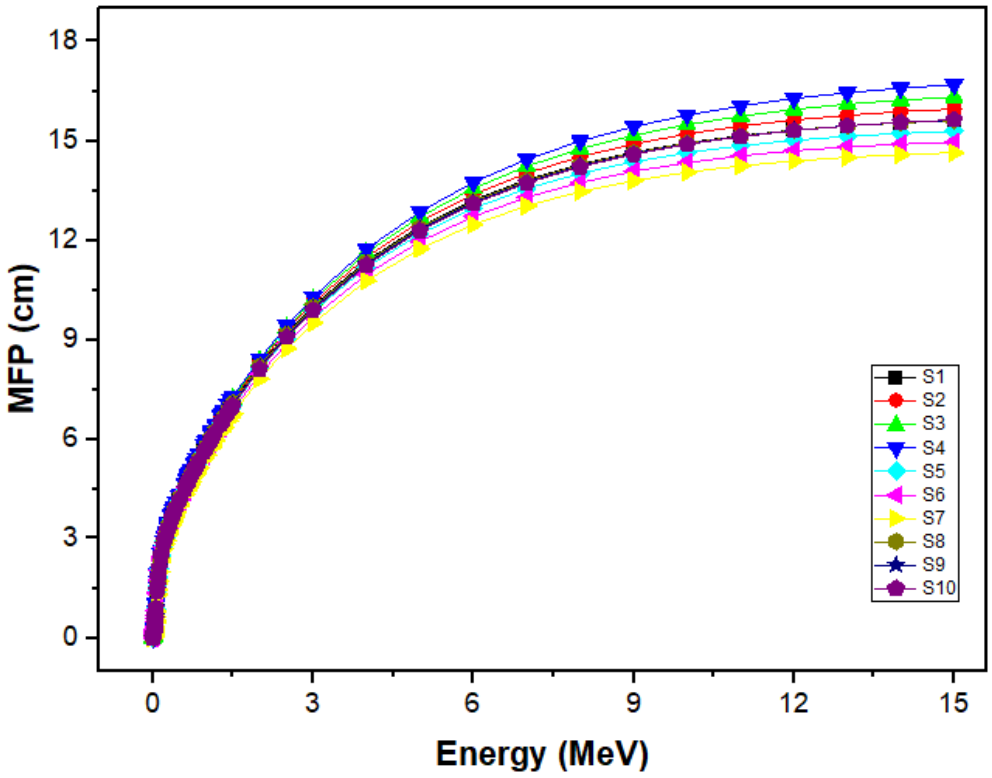


Figure 3. *MFP values of Al 7075 matrix composites reinforced with B_4C and TiB_2 (S1–S10) as a function of photon energy*

TVL

Upon detailed examination of Figure 5, it is observed that while TVL values are quite low for low-energy photons, they rise rapidly as energy increases due to the radiation's enhanced penetration capability. In the high-energy region (where Compton scattering dominates), the curves begin to level off (plateau). Across the entire energy spectrum, the S7 sample (15 wt.% TiB_2) exhibited the lowest TVL values. Titanium's high atomic number and density-enhancing effect have minimized the physical thickness required to block 90% of the radiation by maximizing the material's stopping power.

Since light reinforcements reduce the material's linear attenuation coefficient, a much thicker plate than the S4 sample is required to achieve the same level of shielding. Examination of the TVL graphs reveals that hybrid samples occupy a strategic position among single-reinforced composite materials (B_4C and TiB_2 reinforcements). A comparison of similar studies in literature is given in Table 3.

GU J Sci, Part A | 13(3) 1422-1433 (2026) | 10.54287/gujsa.1999055

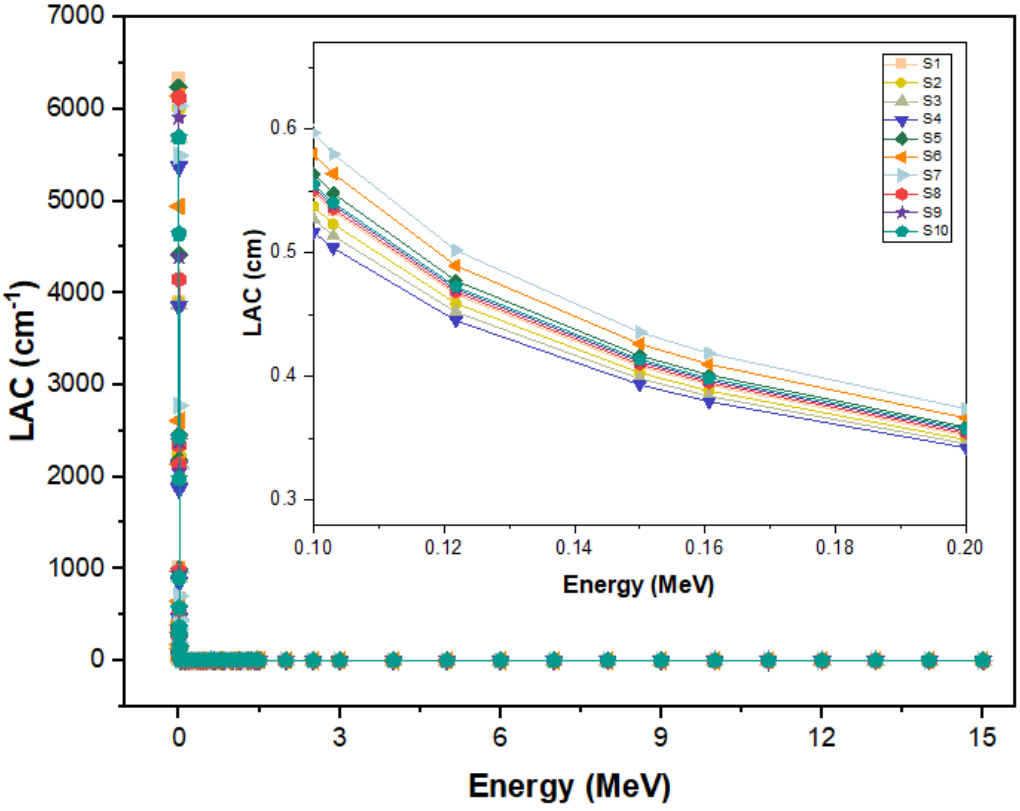


Figure 4. *Al 7075 matrix, B_4C and TiB_2 reinforced composite LAC values of samples (S1–S10) as a function of photon energy*

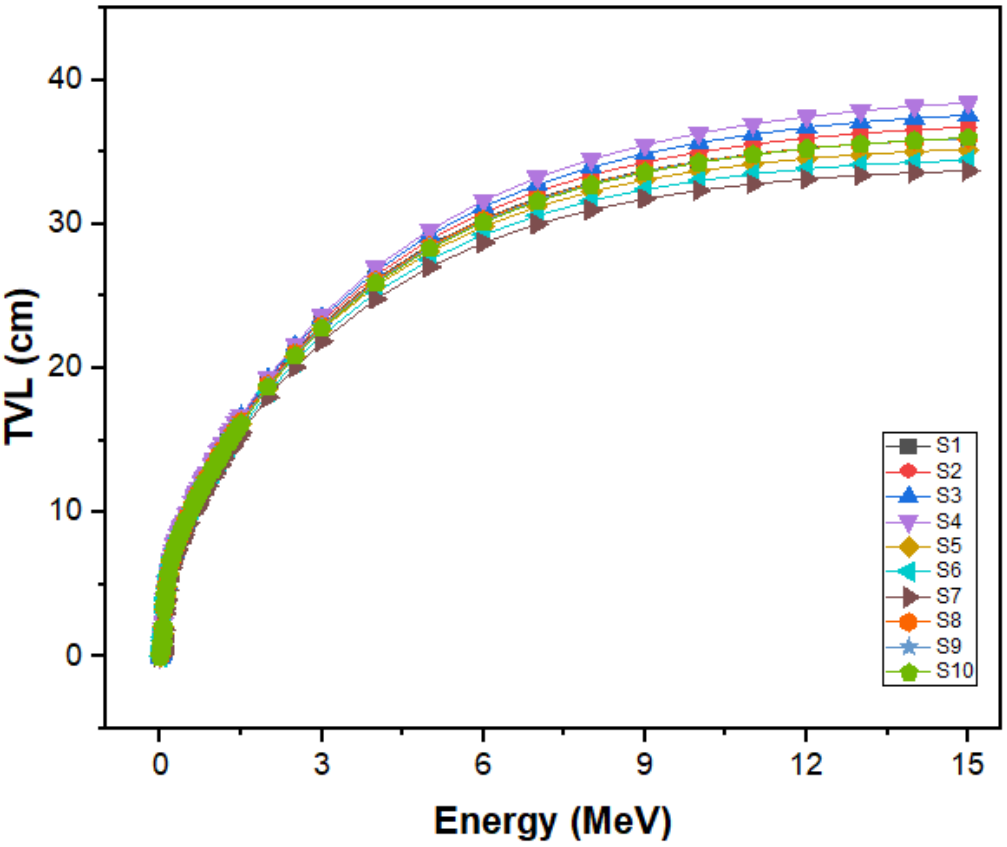


Figure 5. Photon energy dependent TVL values of Al 7075 matrix composites reinforced with B_4C and TiB_2 (S1–S10)

GU J Sci, Part A | 13(3) 1422-1433 (2026) | 10.54287/gujsa.1999055

Table 3. *Similar studies in literature*

Material	Parameters	Values	References
Al alloys	MAC	~0.074 cm^2/g (at 0.662 MeV)	(Sayyed et al., 2018) (Theoretical)
Al-B_4C composites	LAC	~0.14- 0.18 cm^{-1} (at 1.25 MeV)	(Akkas et al., 2015) (Experimental)
Al- B_4C composites	FNRCS	0.06- 0.13 cm^{-1}	(Dai et al., 2013) (Theoretical)
B_4C reinforced Al	TVL	~18- 21 cm (at 1.25 MeV)	(Buyuk et al, 2015) (Experimental)
Al 7xxx series	MAC	~0.075 cm^2/g (at 0.662 MeV)	(Singh & Badiger, 2013) (Theoretical)
S1–S10	MFP	MFP: 0.022- 0.032 cm (at 0.015 MeV)	This Study (Theoretical)
S1–S10	TVL	TVL: 0.115- 0.164 cm (at 0.020 MeV)	This Study (Theoretical)
S1–S10	FNRCS	FNRCS: ~0.080- 0.090 cm^{-1}	This Study (Theoretical)
S1–S10	MAC	0.074-0.075 cm^2/g (at 0.662 MeV)	This Study (Theoretical)
S1–S10	LAC	0.153- 0.166 cm^{-1} (at 1.25 MeV)	This Study (Theoretical)

FNRCS

The FNRCS values for all samples (S1–S10) (Figure 6) indicate that the presence of light elements (particularly boron) is a key factor in neutron shielding. Boron (Z=5) has a very high cross-section for neutron moderation and capture. In this context, as the B_4C ratio increases (from S2 to S4), the neutron-shielding potential of the composites increases.

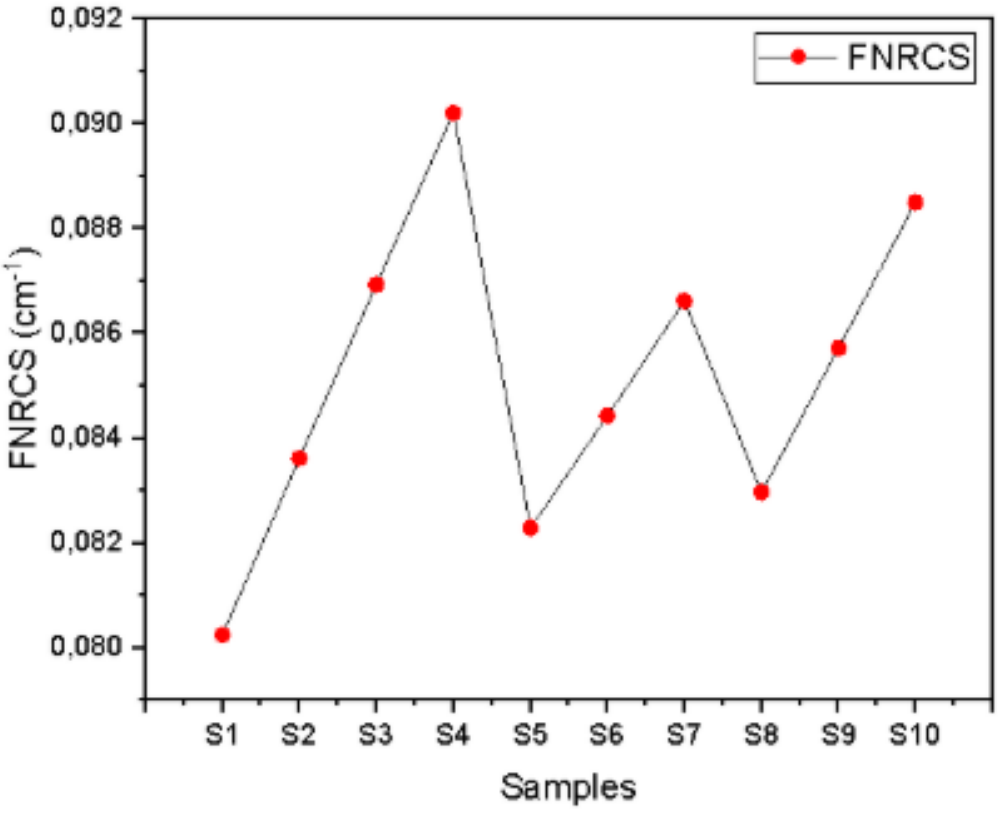


Figure 6. *FNRCS values of Al 7075 matrix composites reinforced with B_4C and TiB_2 (S1–S10)*

GU J Sci, Part A | 13(3) 1422-1433 (2026) | 10.54287/gujsa.1999055

4. CONCLUSION

Theoretical results show that the radiation shielding property of Al 7075 matrix composites is directly related to the ratio, type, and Z-value of the reinforcing phase. Production suitability was considered a fundamental criterion in determining the matrix and reinforcing ratios in the design. The defined ratios were selected considering the technical requirements of the production process, material properties, and production capacity. The observed performance distinctions between the designed samples (S1–S10) were determined as follows:

- It was found that the addition of TiB_2 ceramic to the Al 7075 matrix provided a significant structural advantage. Sample S7, containing 15% TiB_2, exhibited the highest LAC and the lowest TVL values.
- It has been remarked that the addition of B_4C ceramic slightly reduces gamma shielding equate to Al 7075 alloy (S1); this is because of a reduce in the average atomic number of the material.
- Sample S4, including 15% B_4C ceramic, shows the lowest performance in terms of protection against gamma rays, while effective protection requires the highest material thicknesses (MFP and TVL).
- In complex ambiances containing both gamma rays and neutron radiation, the S10, incorporating 7.5% TiB2 + 7.5% B_4C ceramic materials, can be considered the most appropriate engineering resolution.

Thanks to the high strength values and radiation shielding properties of the matrix and reinforcement phases used, these composites offer the possibility of being used as an alternative material in the aerospace industry, medical fields (instead of lead), and the defense industry, especially for electronic warfare systems such as UAVs and AESA radar modules.

AUTHOR CONTRIBUTIONS

Conceptualization, C.Y.; methodology, C.Y., and Z.Ö; validation, C.Y., Z.Ö and U.G; formal analysis, C.Y.; data curation, C.Y.; manuscript–original draft, C.Y., and Z.Ö.; manuscript–review and editing C.Y., U.T., Z.Ö and U.G; visualization, C.Y., and Z.Ö; supervision, U.T. and U.G.

AI Exclusion: Generative AI tools were utilized to assist in the language editing and formatting of this manuscript, in strict accordance with the journal's transparency policies.

Legal Consent: All human authors confirm they have reviewed and legally accepted the final version under the **CC BY-SA 4.0** framework.

ACKNOWLEDGEMENT

No financial support was received.

CONFLICT OF INTEREST

The authors declare no conflict of interest.

GU J Sci, Part A | 13(3) 1422-1433 (2026) | 10.54287/gujsa.1999055

REFERENCES

Agar, O., Sayyed, M. I., Akman, F., Tekin, H. O., & Kaçal, M. R. (2019). An extensive investigation on gamma ray shielding features of Pd/Ag based alloys. *Nuclear Engineering and Technology*, *51*(3), 853–859. https://doi.org/10.1016/j.net.2018.12.014

Akkas, A., Tugrul, A. B., Buyuk, B., Addemir, A. O., Marsoglu, M., & Agacan, B. (2015). Shielding Effect of Boron Carbide Aluminium Metal Matrix Composite against Gamma and Neutron Radiation. *Acta Physica Polonica A*, *128*(2B), B-176-B-179. https://doi.org/10.12693/aphyspola.128.b-176

Akkurt, I., Akyıldırım, H., Mavi, B., Kilincarslan, S., & Basyigit, C. (2010). Photon attenuation coefficients of concrete includes zeolite. *Annals of Nuclear Energy*, *37*(7), 910-914 https://doi.org/10.1016/j.anucene.2010.04.001

Albandar, H. (2019). Basic Modes of Radioactive Decay. In Use of Gamma Radiation Techniques in Peaceful Applications. *IntechOpen*. https://doi.org/10.5772/intechopen.85502

Buyuk, B., Tugrul, A. B., Cengiz, M., Yucel, O., Goller, G., & Sahin, F. C. (2015). Radiation Shielding Properties of Spark Plasma Sintered Boron Carbide-Aluminium Composites. *Acta Physica Polonica A*, *128*(2B), B-132-B-134. https://doi.org/10.12693/aphyspola.128.b-132

Canakci, A., & Arslan, F. (2012). Abrasive wear behaviour of B_4C particle reinforced Al2024 MMCs. The International *Journal of Advanced Manufacturing Technology*, *63*(5–8), 785–795. https://doi.org/10.1007/s00170-012-3931-8

Chen, C., Li, B., Wang, Y., Bian, M., Kang, X., & Yang, X. (2025). Recent Advances on Aluminum-Based Boron Carbide Composites: Performance, Fabrication, and Applications. *Materials*, *18*(23), 5469. https://doi.org/10.3390/ma18235469

Dai, C.-J., Liu, X.-Q., Liu, Z.-L., & Liu B.-L. (2013). The Monte Carlo simulation of neutron shielding performance of boron carbide reinforced with aluminum composites. *Acta Physica Sinica*, *62*(15), 152801. https://doi.org/10.7498/aps.62.152801

El-Khayatt, A. M. (2010). Calculation of fast neutron removal cross-sections for some compounds and materials. *Annals of Nuclear Energy*, *37*(2), 218-222. https://doi.org/10.1016/j.anucene.2009.10.022

Heinz, A., Haszler, A., Keidel, C., Moldenhauer, S., Benedictus, R., & Miller, W. S. (2000). Recent development in aluminium alloys for aerospace applications. *Materials Science and Engineering: A*, *280*(1), 102-107. https://doi.org/10.1016/S0921-5093(99)00674-7

Hubbell, J. H., & Seltzer, S. M. (1995). Tables of X-ray Mass Attenuation Coefficients and Mass Energy-Absorption Coefficients 1 keV to 20 MeV for Elements Z = 1 to 92 and 48 Additional Substances of Dosimetric Interest. National Institute of Standards and Technology, NISTIR 5632. https://doi.org/10.6028/NIST.IR.5632

Hubbell, J. H., & Seltzer, S. M. (2004). Tables of X-ray Mass Attenuation Coefficients and Mass Energy-Absorption Coefficients 1 keV to 20 MeV for Elements Z = 1 to 92 and 48 Additional Substances of Dosimetric Interest. NIST Standard Reference Database 126. https://doi.org/10.18434/T4D01F

Knoll, G. F. (2010). *Radiation Detection and Measurement* (4th Ed.). John Wiley & Sons, New York.

Miller, W. S., Zhuang, L., Bottema, J., Wittebrood, A. J., De Smet, P., Haszler, A., & Vieregge, A. (2000). Recent development in aluminium alloys for the automotive industry. *Materials Science and Engineering: A*, *280*(1), 37-49. https://doi.org/10.1016/S0921-5093(99)00653-X

Şakar, E., Özpolat, Ö. F., Alım, B., Sayyed, M. I., & Kurudirek, M. (2020). Phy-X / PSD: Development of a user-friendly online software for calculation of parameters relevant to radiation shielding and dosimetry. *Radiation Physics and Chemistry*, *166*, 108496. https://doi.org/10.1016/j.radphyschem.2019.108496

Sayyed, M. I., Akman, F., Kumar, A., & Kaçal, M. R. (2018). Evaluation of radioprotection properties of some selected ceramic samples. *Results in Physics*, *11*, 1100–1104. https://doi.org/10.1016/j.rinp.2018.11.028

Shackelford, J. F., & Alexander, W. (Eds.) (2001). CRC Materials Science and Engineering Handbook (3rd Ed.). CRC Press, Boca Raton, FL.

Singh, V. P., & Badiger, N. M. (2013). Study of mass attenuation coefficients, effective atomic numbers and electron densities of carbon steel and stainless steels. *Radioprotection*, *48*(3), 431–443. https://doi.org/10.1051/radiopro/2013067

Starke, E. A., & Staley, J. T. (2011). Application of modern aluminum alloys to aircraft. In: R. Lumley (Eds.), *Fundamentals of Aluminium Metallurgy. Production, Processing and Applications* (pp. 747-783). Woodhead Publishing, Cambridge. https://doi.org/10.1533/9780857090256.3.747

Toptan, F., Kilicarslan, A., Karaaslan, A., Cigdem, M., & Kerti, I. (2010). Processing and microstructural characterization of AA 1070 and AA 6063 matrix B4C particle reinforced composites. *Materials & Design*, *31*, S87-S91. https://doi.org/10.1016/j.matdes.2009.11.064

Williams, J. C., & Starke, E. A., Jr. (2003). Progress in structural materials for aerospace systems. In: S. Suresh (Eds.), The Golden Jubilee Issue. Selected topics in Materials Science and Engineering: Past, Present and Future. *Acta Materialia*, *51*(19), 5775–5799. https://doi.org/10.1016/j.actamat.2003.08.023

Wood, J. (1982). *Computational Methods in Reactor Shielding*. Pergamon Press.